

1 **A New Simplified Parameterization of Secondary Organic Aerosol in**  
2 **the Community Earth System Model Version 2 (CESM2; CAM6.3)**

3 Duseong S. Jo<sup>1</sup>, Simone Tilmes<sup>1</sup>, and Louisa K. Emmons<sup>1</sup>, Siyuan Wang<sup>2,3</sup>, Francis Vitt<sup>1</sup>

4 <sup>1</sup>National Center for Atmospheric Research, Boulder, CO, USA

5 <sup>2</sup>Cooperative Institute for Research in Environmental Sciences, University of Colorado, Boulder, CO, USA

6 <sup>3</sup>NOAA Chemical Sciences Laboratory, Boulder, CO, USA

7

8

9

10

11

12

13

*Correspondence to:* Duseong S. Jo (cdswk@ucar.edu)

14

15

16

17

Manuscript submitted to Geoscientific Model Development

18 **Abstract.** The Community Earth System Model (CESM) community has been providing versatile  
19 modeling options, with simple to complex chemistry and aerosol schemes in a single model, in order to  
20 support the broad scientific community with various research interests. While different model  
21 configurations are available in CESM and these can be used for different fields of Earth system science,  
22 simulation results that are consistent across configurations are still desirable. Here we develop a new  
23 simple secondary organic aerosol (SOA) scheme in the Community Atmosphere Model (CAM) version  
24 6.3, the atmospheric component of the CESM. The main purpose of this simplified SOA scheme is to  
25 reduce the differences in aerosol concentrations and radiative fluxes between CAM and CAM with  
26 detailed chemistry (CAM-chem) while maintaining the computational efficiency of CAM. CAM  
27 simulation results using the default CAM6 and the new SOA schemes are compared to CAM-chem results  
28 as a reference. More consistent SOA concentrations are obtained globally when using the new SOA  
29 scheme, for both temporal and spatial variabilities. The new SOA scheme shows 62% of grid cells  
30 globally are within a factor of 2 compared to the CAM-chem SOA concentrations, which is improved  
31 from 24% when using the default CAM6 SOA scheme. Furthermore, other carbonaceous aerosols (black  
32 carbon and primary organic aerosol) in CAM6 become closer to CAM-chem results, due to more similar  
33 microphysical aging time scales influenced by SOA coating, which in turn leads to comparable wet  
34 deposition fluxes. This results in an improved global atmospheric burden and concentrations at the high  
35 latitudes of the Northern Hemisphere compared to the full chemistry version (CAM-chem). As a  
36 consequence, the radiative flux differences between CAM-chem and CAM in the Arctic region (up to 6  
37  $\text{W m}^{-2}$ ) are significantly reduced for both nudged and free-running simulations. We find that the CAM6  
38 SOA scheme can still be used for radiative forcing calculation as the high biases exist both in pre-  
39 industrial and present conditions, but studies focusing on the instantaneous radiative effects would benefit  
40 from using the SOA scheme developed in this study. The new SOA scheme also has technical advantages  
41 including the use of identical SOA precursor emissions as CAM-chem from the online biogenic  
42 emissions, instead of pre-calculated emissions that may introduce differences. Future parameter updates  
43 on the CAM-chem SOA scheme can be easily translated to the new CAM SOA scheme as it is derived  
44 from the CAM-chem SOA scheme.

45 **Short Summary.** The new simple secondary organic aerosol (SOA) scheme has been developed for the  
46 Community Atmosphere Model (CAM), based on the complex SOA scheme in CAM with detailed  
47 chemistry (CAM-chem). The CAM with the new SOA scheme shows better agreements with CAM-chem  
48 in terms of aerosol concentrations and radiative fluxes, which ensures more consistent results between  
49 different compsets in the Community Earth System Model. The new SOA scheme also has technical  
50 advantages for future developments.

## 51 **1 Introduction**

52 Secondary organic aerosol (SOA) accounts for a substantial fraction of ambient tropospheric aerosol  
53 (Hallquist et al., 2009). Atmospheric models generally use parameterizations to simulate SOA because it  
54 is composed of a wide range of different organic molecules (Goldstein and Galbally, 2007) and due to  
55 limited knowledge of SOA formation in the atmosphere (Nault et al., 2021). The SOA parameterization  
56 in 3D atmospheric chemistry models varies from the simple method of multiplying constant yields to  
57 emissions, to the rather complex volatility basis set (VBS) approach (Donahue et al., 2006, 2011, 2012;  
58 Jimenez et al., 2009), which considers the oxidation of volatile organic compounds (VOCs) and gas-  
59 particle partitioning, as shown in the recent model intercomparison study for organic aerosol (OA)  
60 (Hodzic et al., 2020).

61 Climate models that have to perform hundreds of years of simulations and many ensemble members  
62 often use very simple parameterizations to calculate SOA in the model (Tsigaridis and Kanakidou, 2018),  
63 due to the high computational cost associated with chemistry, deposition, and the increased number of  
64 model tracers to be transported (Jo et al., 2019). Because SOA affects climate through aerosol-radiation  
65 and aerosol-cloud interactions, and climate also affects SOA through changing biogenic emissions and  
66 photochemistry (Gettelman et al., 2019a; Sporre et al., 2019; Tilmes et al., 2019; Jo et al., 2021), the  
67 accurate representation of SOA in climate models is important but needs to have low computational cost  
68 for long-term simulation purposes.

69 The Community Earth System Model Version 2 (CESM2) has two different SOA schemes, one  
70 simplified scheme for the Community Atmosphere Model (CAM) version 6 (Danabasoglu et al., 2020)  
71 and the Whole Atmosphere Community Climate Model (WACCM) version 6 with the Middle  
72 Atmosphere (MA) chemistry (Gettelman et al., 2019b), and a VBS scheme for the CAM6 with  
73 comprehensive chemistry (CAM6-chem) (Emmons et al., 2020) and the WACCM6 with the TSMLT  
74 (troposphere, stratosphere, mesosphere, and lower thermosphere) mechanism. For the purpose of climate  
75 studies using many ensemble members, CAM6 is generally used for computational efficiency. Models  
76 like WACCM6 with TSMLT are used for detailed chemistry and aerosol studies, but in general, only a  
77 few ensemble members can be performed. Ideally, the two SOA schemes in simple and complex  
78 chemistry configurations should give the same results to maintain model consistency regarding aerosol

79 fields and resulting climate forcings, but the spatial and temporal distributions of SOA between CAM and  
80 CAM-chem (and WACCM TSMLT) are different enough to have a significant effect on black carbon  
81 (BC) and the Earth's radiation budget (Tilmes et al., 2019).

82 Here we propose a new simplified and computationally affordable SOA scheme for CAM, which is  
83 based on the VBS scheme in CAM-chem. We compare three SOA schemes (VBS, simplified SOA  
84 scheme in CAM6, and the new CAM SOA scheme in this study) under a few different CESM2  
85 configurations (specified dynamics and free-running in preindustrial and present conditions). The new  
86 approach substantially reduces the differences in aerosol and radiation values between CAM and CAM-  
87 chem (Sect. 3). The new SOA scheme also has a technical advantage as it does not need input files for  
88 the SOA precursor, but uses the same emissions files as CAM-chem or WACCM for individual SOA  
89 precursor species (isoprene, terpenes, toluene, etc.).

90

## 91 **2 Method**

92 In this section, we present SOA schemes in CAM-chem and CAM, along with the new simplified  
93 SOA scheme, as summarized in Fig. 1 and Table 1. General descriptions for other carbonaceous aerosols  
94 (BC and primary organic aerosol (POA)) are also explained as concentrations of those carbonaceous  
95 aerosols are affected by SOA concentrations (Tilmes et al., 2019). This section also includes the  
96 simulation set-up for comparisons between SOA schemes in Sect 3. To facilitate discussion throughout  
97 the paper, the existing SOA scheme used in CAM is denoted as "CAM6", and the newly developed SOA  
98 scheme in this paper is denoted as "CAM (This study)."

99

100

101 **Table 1.** SOA schemes used in this study. Computational costs are estimated on the Cheyenne  
 102 supercomputer at NCAR. Computational cost ranges are given in parentheses with the average value.

SOA scheme	CAM-chem	CAM6	CAM (This study)
Emissions	Individual VOCs, online biogenic emissions	Pre-calculated, lumped SOAG emissions	Individual VOCs, online biogenic emissions
VOCs and chemistry	explicitly simulated	No	Lumped tracer (SOAE) with 1-day lifetime
Number of SOA bins	5	1	1
Saturation vapor pressure ( $\mu\text{g m}^{-3}$ )	0.01, 0.1, 1, 10, 100	1.02	1
Enthalpy of vaporization ( $\text{kJ mol}^{-1}$ )	153, 142, 131, 120, 109	156	131
SOA yield	Based on the VBS	Fixed fraction and scaled up by 50%	Based on the VBS but lumped
Loss processes	wet & dry deposition of SOAG photolytic loss of soa	No deposition of SOAG No photolytic loss	wet & dry deposition of SOAG photolytic loss of soa
Effective Henry's law constants of SOAG ( $\text{M atm}^{-1}$ )	$4.0 \times 10^{11}$ , $3.2 \times 10^{10}$ , $1.6 \times 10^9$ , $3.2 \times 10^8$ , $1.6 \times 10^7$	N/A	$1.6 \times 10^9$
Computational cost (pe-hrs / simulated_year)	7933 (7783 - 8083)	2398 (2353 - 2448)	2455 (2414 - 2501)

103

104

105

106

107

108

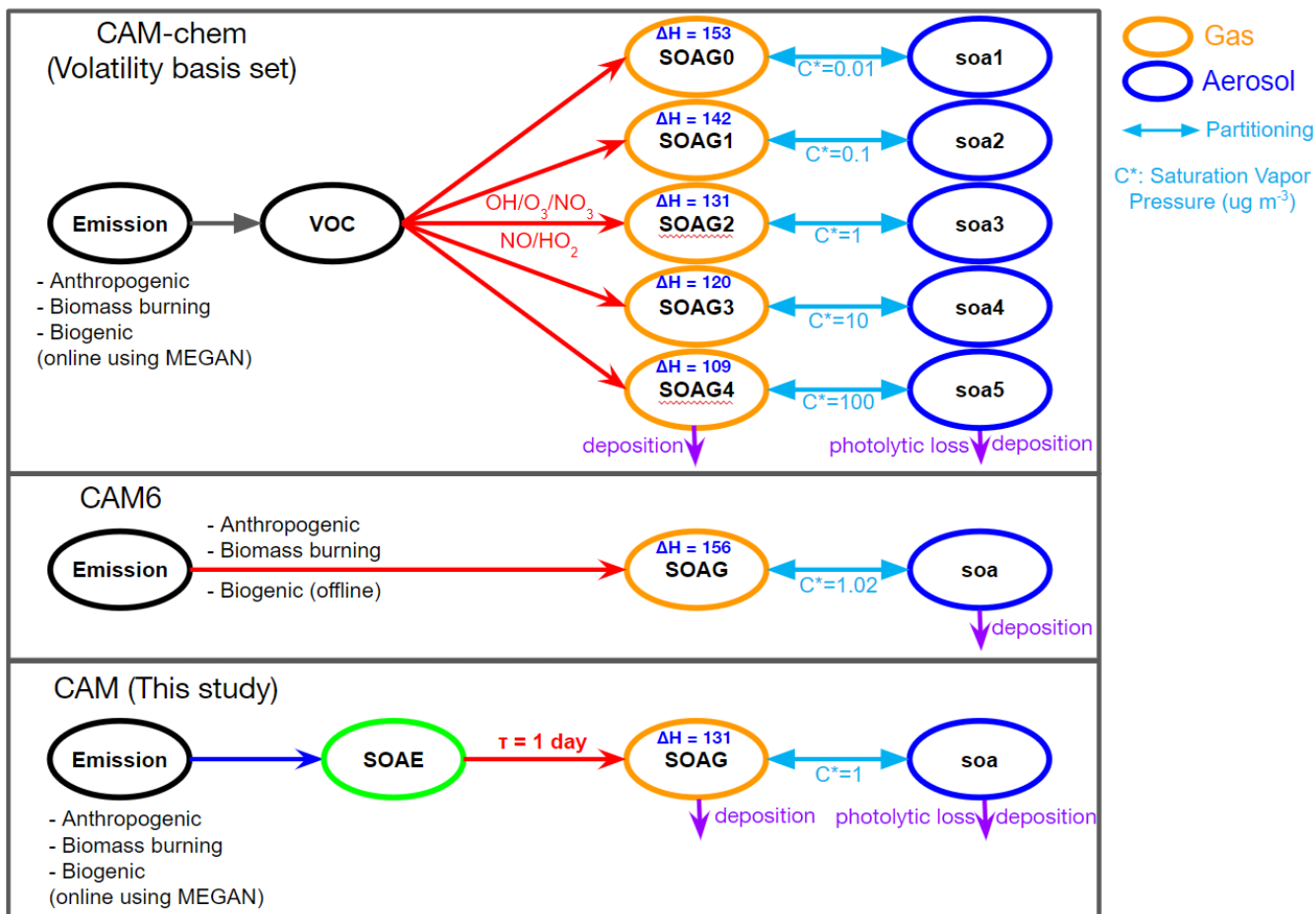


**Figure 1.** The notations are based on variable names used in CESM2. Note that "SOAG" begins with 0, while "soa" starts with 1 in CAM-chem (Tilmes et al., 2019; Emmons et al., 2020). In CESM2, gases are written in upper case and aerosols are written in lower case.

## 2.1 SOA scheme in CAM-chem

SOA in CAM-chem is simulated using the VBS approach, as described by Tilmes et al. (2019). The VBS scheme in CAM-chem incorporates recent findings such as wall-corrected SOA yields, photolytic removal of SOA, and more efficient removal by dry and wet deposition. Details can be found in Hodzic et al. (2016). The VBS approach in CAM-chem has been evaluated against surface and aircraft observations in the United States, Europe, East Asia, the Amazon, and remote atmosphere (Hodzic et al.,

120 2016, 2020; Tilmes et al., 2019; Jo et al., 2021; Oak et al., 2022). Here we briefly describe the  
121 characteristics that can be compared to the simple SOA scheme in CAM.

122 CAM-chem uses a VBS scheme with 5 volatility bins (see Fig. 1) with saturation vapor pressures  
123 spanning from 0.01 to 100  $\mu\text{g m}^{-3}$  at 300K. Enthalpy of vaporization values are 153, 142, 131, 120, and  
124 109  $\text{kJ mol}^{-1}$  for 0.01, 0.1, 1, 10, and 100  $\mu\text{g m}^{-3}$ , respectively, at 300K based on Epstein et al. (2010).  
125 Traditional SOA precursors such as isoprene, monoterpenes, sesquiterpenes, benzene, toluene, and  
126 xylenes are explicitly simulated in the model, and the oxidation of those VOCs with OH, O<sub>3</sub>, and NO<sub>3</sub>  
127 makes gas phase semivolatiles (SOAG) that are in equilibrium with SOA according to the volatility bins.  
128 VOCs and oxidants are not consumed to avoid duplication, as VOC chemistry is separately simulated in  
129 CAM-chem (Jo et al., 2021). Semi- and intermediate-range volatility organic compounds (S/IVOCs) are  
130 also considered with a bimolecular OH reaction. Since S/IVOCs are defined by volatility and exact  
131 chemical speciation is not available for them, 60% of POA and 20% of total non-methane VOC  
132 (NMVOC) emissions are assumed to be SVOCs and IVOCs, respectively (Hodzic et al., 2016). Biogenic  
133 VOCs are calculated online using the Model of Emissions of Gases and Aerosols from Nature (MEGAN)  
134 version 2.1 (Guenther et al., 2012) available in the Community Land Model (CLM) version 5, a  
135 component of CESM and coupled to CAM (Lawrence et al., 2019). Photolytic removal of SOA is  
136 calculated as 0.04% of the NO<sub>2</sub> photolysis rate (Hodzic et al., 2016). Heterogeneous loss of SOA is not  
137 included in CAM-chem (Tilmes et al., 2019). However, the effect of heterogeneous removal on SOA  
138 burden is small (lifetime of 80-90 days) compared to the rapid loss of SOA due to photolysis (Hodzic et  
139 al., 2016).

140 CAM-chem also supports an extended VBS compset that keeps track of VBS tracers from three  
141 sources (anthropogenic, biomass burning, and biogenic), leading to 15 SOA species simulated in total.  
142 This option is not generally used except for studies tracking sources of SOA, as total SOA burden and  
143 formation are very similar between the two options because the same volatility bins are used (Tilmes et  
144 al., 2019).

145 In terms of aerosol modes, the four-mode version of the Modal Aerosol Module (MAM4) is generally  
146 used in recent scientific applications (Liu et al., 2016). MAM4 is a 2-moment scheme that includes  
147 interstitial and cloud-borne aerosols and considers Aitken, accumulation, coarse, and primary carbon



148 modes. The standard deviation of each mode is fixed, but the wet radius in each mode can change per  
149 grid box, depending on the composition. Aitken mode mass grows into the accumulation mode, and  
150 accumulation mode mass grows into the coarse mode. More details are provided in Liu et al. (2012) and  
151 (2016). SOA is simulated using Aitken and accumulation modes but most of the mass (>99%) is in the  
152 accumulation mode (Tilmes et al., 2019). In total, 15 tracers (5 for the gas phase and 10 for the aerosol  
153 phase - 5 bins  $\times$  2 modes) are used for the SOA calculation in CAM-chem.

## 154 **2.2 SOA scheme in CAM6**

155 The simplified SOA scheme in CAM6 uses 3 tracers (1 for the gas phase and 2 for the aerosol phase).  
156 Like the VBS, both gas-phase (SOAG) and aerosol-phase (soa\_a1 and soa\_a2 for accumulation and  
157 Aitken modes) are simulated with gas-aerosol partitioning, with the enthalpy of vaporization of 156 kJ  
158 mol<sup>-1</sup> and the saturation vapor pressure of 1.02  $\mu\text{g m}^{-3}$  (Liu et al., 2012). SOAG does not undergo dry and  
159 wet removal, which is also different from the VBS that calculates dry and wet deposition of gas-phase  
160 semivolatiles (SOAGs). Note that dry and wet deposition are applied to SOA in all simulation cases as  
161 shown in Fig 1.

162 Unlike the VBS representation which explicitly simulates parent VOCs, this scheme does not  
163 simulate the chemistry of VOCs but uses pre-calculated emissions using fixed mass yields for the  
164 following VOC categories: 5% BIGALK (lumped  $\geq\text{C}_4$  alkanes), 5% BIGENE (lumped  $\geq\text{C}_4$  alkenes),  
165 15% aromatics, 4% isoprene, and 25% monoterpenes (Liu et al., 2012). For biogenic VOCs, offline  
166 emissions are precalculated and provided as an additional input file based on biogenic emissions  
167 simulated by CLM-MEGAN2.1. Generally, the offline biogenic VOC emission does not have annual  
168 variations and is repeated over the simulation period. Note that those SOAG emissions are further  
169 increased by 50% after model tuning involving the aerosol indirect effect (Liu et al., 2012).

## 170 **2.3 New SOA scheme in CAM**

171 The SOA scheme developed in this study uses a similar approach to the SOA scheme in CAM6, but  
172 several modifications have been made to allow more consistent results with the VBS scheme in CAM-  
173 chem (Fig. 1). First, VOC species that generate SOA are matched to the VBS. In other words, BIGALK

174 and BIGENE are no longer used for the calculation of SOA emissions, and instead, sesquiterpenes and  
175 S/IVOCs are considered for calculating the interactive emissions of SOA. This change can be  
176 scientifically justified because SOA yields generally increase with the carbon number (Lim and Ziemann,  
177 2009; Srivastava et al., 2022). BIGALK and BIGENE are mainly composed of C4-C6 alkanes and alkenes  
178 (Emmons et al., 2020), but S/IVOCs correspond to C12 or higher n-alkanes (Robinson et al., 2007).

179 Second, VBS product yields (forming semi-volatile compounds in the model, sum of gas and aerosol  
180 phases, and used for the interactive emissions) have been calculated based on the CAM-chem yields,  
181 which were adapted from Hodzic et al. (2016). The VBS product yields for the first four bins and 20% of  
182 the fifth bin are summed up for each compound. Only 20% of the fifth bin yield is used, as it is the most  
183 volatile bin and its saturation vapor pressure is 100 times higher than the volatility bin we use in CAM  
184 (Fig. 1). We selected 20% based on the SOA burden comparison between CAM-chem and CAM, by  
185 adjusting this fraction with multiple simulation tests. We consider VBS product yields from OH reactions  
186 only in this calculation, because the reaction with OH is dominant for VOCs. Only low NO<sub>x</sub> yields are  
187 used in this study which is consistent with Tilmes et al. (2019), which is appropriate for global climate  
188 studies with 1° horizontal resolution of the model grid. For air quality studies with high spatial resolution,  
189 CAM-chem with NO<sub>x</sub>-dependent SOA yields can be used (Schwantes et al., 2022). The resulting yields  
190 derived from CAM-chem results are 0.28, 0.64, 0.04, 0.16, 0.45, 0.35, 0.41, and 0.80 for monoterpenes,  
191 sesquiterpenes, isoprene, benzene, toluene, xylenes, IVOC, and SVOC, respectively. These yields are  
192 constants and do not change during the run, as in CAM-chem. It is worth noting that those yields can be  
193 easily updated in the CAM run-time namelist file if there is a future update to the CAM-chem VBS  
194 scheme.

195 Third, we add a new tracer called “SOAE” (Fig. 1) to consider the time that VOCs and intermediate  
196 chemical species undergo oxidation before forming semivolatiles. We assume a constant 1-day e-folding  
197 lifetime to convert “SOAE” to “SOAG” which can be partitioned into aerosols so that oxidant fields do  
198 not have to be simulated in CAM for computational efficiency. The 1-day lifetime corresponds to the OH  
199 reaction rate constant of  $10^{-11} \text{ cm}^3 \text{ molecules}^{-1} \text{ s}^{-1}$  with a global annual mean OH concentration of  $11.6 \times$   
200  $10^5 \text{ molecules cm}^{-3}$  (Warneck and Williams, 2014).

201 Fourth, parameters are adjusted for consistency with the VBS scheme. The enthalpy of vaporization  
202 is changed from 156 to 131 kJ mol<sup>-1</sup>, which is the value used in the third bin of the VBS scheme. This  
203 can change SOA in the upper troposphere where temperature dependency becomes important. Deposition  
204 of gas phase semivolatiles (SOAG) and the photolytic reaction of SOA are also added (deposition of SOA  
205 is already considered in CAM6), which can affect SOA concentrations in the remote atmosphere.  
206 Saturation vapor pressure change with the assumption of 10% of POA as oxygenated (Liu et al., 2012) is  
207 not used in this scheme for consistency with the VBS scheme.

208 Fifth, the same offline emission files (anthropogenic and biomass burning) and online emission  
209 (biogenic) are used as the VBS method in CAM-chem, via namelist control. As a result, preprocessing  
210 for SOAG emission is no longer needed, and annual variability as well as the diurnal cycle for biogenic  
211 emission can be easily considered. Note that biogenic emission is always calculated in CLM, regardless  
212 of whether the emission is used or not in CAM or CAM-chem. Therefore, using online biogenic emissions  
213 does not add computational cost.

## 214 **2.4 Other carbonaceous aerosols**

215 Here we describe BC and POA simulations in CAM and CAM-chem, as those are affected by SOA  
216 concentrations through microphysics. Because BC, POA, and SOA precursors are emitted from the same  
217 sources (except for the biogenic SOA), changes in one component can significantly affect other  
218 components. Tilmes et al. (2019) reported ~20% differences between the simplified SOA and the VBS  
219 scheme in terms of the global burden of BC and POA, while the difference for the sulfate burden was  
220 very small (< 1%).

221 Unlike SOA, there is no difference in BC and POA simulation schemes between CAM and CAM-  
222 chem, because BC and POA are chemically inert and the standard aerosol module is the same (MAM4)  
223 for both CAM and CAM-chem. However, BC and POA can change through the following processes.  
224 Both POA and BC are emitted into the primary carbon mode, where they are coated by sulfate and SOA,  
225 and then transferred into the accumulation mode and slowly aged through condensation and coagulation,  
226 with a threshold coating thickness of eight hygroscopic monolayers of SOA (Liu et al., 2016). In the  
227 accumulation mode, aerosols are hydrophilic, with a volume-weighted hygroscopicity calculated based

228 on the volume mixing rule. A strong increase in SOA formation over source regions, which is true for  
229 CAM-chem SOA based on Hodzic et al. (2016) SOA scheme, increases the internally mixed aerosol  
230 number, which causes enhanced aging of BC and POA. As a result, the CAM SOA scheme simulates  
231 more than two times higher primary carbon mode concentrations of BC and POA through reduced aging,  
232 but ~10% lower accumulation mode concentrations of both. This results in increased dry deposition and  
233 decreased wet deposition in the CAM SOA scheme compared to the CAM-chem SOA scheme, as the  
234 primary carbon mode is hydrophobic but the accumulation mode is hydrophilic in CESM. More details  
235 can be found in Tilmes et al. (2019).

236

## 237 **2.5 Simulation set-up**

238 We conduct three types of model experiments for different application scenarios using the  
239 development version of CESM2.2 or CAM6.3 (tag name: cam6\_3\_050). First, a specified dynamics run  
240 is performed for the analysis of the present condition using the nudged meteorological fields. Temperature  
241 and horizontal winds are nudged towards the Modern-Era Retrospective analysis for Research and  
242 Applications version 2 (MERRA2) every 3 hours (Gelaro et al., 2017). In this simulation, we run the  
243 model for the year 2013 with a spin-up period of one year. Second, historical runs are performed for the  
244 1850s and 2000s with prescribed sea surface temperatures and sea ice conditions. These are free-running  
245 simulations for 12 years for each condition with the two years discarded for the spin-up. In this case, the  
246 CLM is run with the satellite phenology (SP) option which uses a prescribed leaf area index (LAI) based  
247 on MODIS satellite observations (Lawrence et al., 2019). In this option, the input LAI value for each  
248 plant functional type (PFT) is the same between the 1850s and 2000s but the PFT fraction changes with  
249 time. As a result, the final LAI used for biogenic emission calculation is slightly different between the  
250 two periods. The third is the same as the second experiment, but the vegetation state including LAI is  
251 simulated prognostically by CLM (biogeochemistry; BGC) (Lawrence et al., 2019). In addition to  
252 absolute values, the difference between the 1850s and 2000s is investigated from the historical simulations  
253 in Sect. 3.3, to compare simulation results in terms of the radiative forcing.

254 In all simulations, the bi-directional oceanic flux of dimethyl sulfide (DMS) is calculated using the  
255 Online Air-Sea Interface for Soluble Species (OASISS) (Wang et al., 2019, 2020) and the climatological  
256 surface seawater DMS concentration (Lana et al., 2011), which will be the default DMS emission in the  
257 next CESM version. In brief, OASISS determines the direction and the magnitude of the ocean fluxes  
258 based on solubility, the physical conditions in the ocean (e.g., sea surface temperature, salinity, waves  
259 and bubbles) and the atmosphere (temperature, wind). Figure S1 shows the timeseries comparisons  
260 between online DMS emissions calculated by OASISS and offline DMS emissions that have been used  
261 in CAM-chem (Emmons et al., 2020). For the Northern Hemisphere winter, both emissions show similar  
262 magnitudes, but there are approximately a factor of two differences between the two emissions in other  
263 seasons. Annual mean DMS fluxes for the 1850s and 2000s are 21.6 and 22.2 TgS yr<sup>-1</sup> when calculated  
264 by OASISS, but are 13.8 and 13.9 TgS yr<sup>-1</sup> from the offline emissions. OASISS DMS emission flux is  
265 much closer to the recent global DMS emission estimates (27.1 TgS yr<sup>-1</sup>) by Hulswar et al. (2022).

266 Dry deposition of aerosols is calculated using the Zhang et al. (2001) parameterization as described  
267 in Liu et al. (2012), while gas-phase compounds are dry deposited based on a resistance-based  
268 parameterization as described in Emmons et al. (2020). In CAM6, in-cloud removal in shallow convective  
269 and stratiform clouds is calculated based on the cloud and precipitation information from the MG2  
270 microphysics scheme (Gettelman and Morrison, 2015). For wet removal in deep convective clouds,  
271 CAM6 uses the Zhang and McFarlane (1995) deep convection scheme, coupled with a unified scheme  
272 for aerosol convective transport and wet scavenging by Wang et al. (2013) with subsequent updates and  
273 improvements by Shan et al. (2021). The convective-cloud activation fractions, which are used to  
274 calculate convective in-cloud scavenging of aerosols, are set to 0.0 for the primary carbon mode and 0.8  
275 for Aitken and accumulation modes of carbonaceous aerosols (Liu et al., 2012). Wet deposition of gaseous  
276 compounds is based on Neu and Prather (2012) with modifications by Emmons et al. (2020).

277

278

279 **3 Results**

280 In this section, the SOA scheme in CAM6 and the SOA scheme developed in this study are evaluated  
 281 against CAM-chem as a reference. As SOA changes can affect the other carbonaceous aerosols and  
 282 radiation fields in CESM2 (Tilmes et al., 2019), we also compare those simulation fields as shown in  
 283 Table 2.

284 **Table 2.** Global annual mean burden of carbonaceous aerosols (SOA, SOAG (semivolatiles that are in  
 285 equilibrium with particle phase SOA), BC, and POA) and radiation fields (FSNT (net shortwave flux at  
 286 top of model), FLNT (net longwave flux at top of model), top of the atmosphere (TOA) imbalance, SWCF  
 287 (shortwave cloud forcing), LWCF (longwave cloud forcing)). Because CAM uses the offline biogenic  
 288 SOA emissions, SOA in the default CAM is not affected by the CLM option (Sect. 2.5). Units are Gg for  
 289 aerosols and  $W m^{-2}$  for radiation fields.

Simulation	SOA scheme	SOA	SOAG	BC	POA	FSNT	FLNT	TOA imbalance	SWCF	LWCF
2013 (Nudged)	CAM-chem	1022	484	117	587	236.7	238.7	-2.0	-50.5	22.2
	CAM6	948	118	131	704	237.7	239.2	-1.5	-49.6	21.7
	CAM (This study)	1027	129	111	574	237.3	239.3	-2.0	-49.8	21.6
1850s (SP)	CAM-chem	780	367	31	299	232.3	235.0	-2.7	-54.6	26.3
	CAM6	699	102	43	435	233.1	235.4	-2.3	-53.7	25.7
	CAM (This study)	747	94	30	300	232.7	235.3	-2.7	-54.0	25.7
2000s (SP)	CAM-chem	793	375	89	510	231.3	234.0	-2.7	-56.1	25.7
	CAM6	796	102	102	635	232.0	234.4	-2.4	-55.3	25.1
	CAM (This study)	744	105	83	488	231.7	234.4	-2.7	-55.6	25.1
1850s (BGC)	CAM-chem	826	357	31	302	232.2	235.0	-2.8	-55.0	26.4
	CAM (This study)	770	89	31	304	232.6	235.3	-2.7	-54.3	25.9
2000s (BGC)	CAM-chem	982	411	88	510	231.3	234.0	-2.7	-56.3	25.8
	CAM (This study)	952	109	83	490	231.6	234.3	-2.7	-55.8	25.2

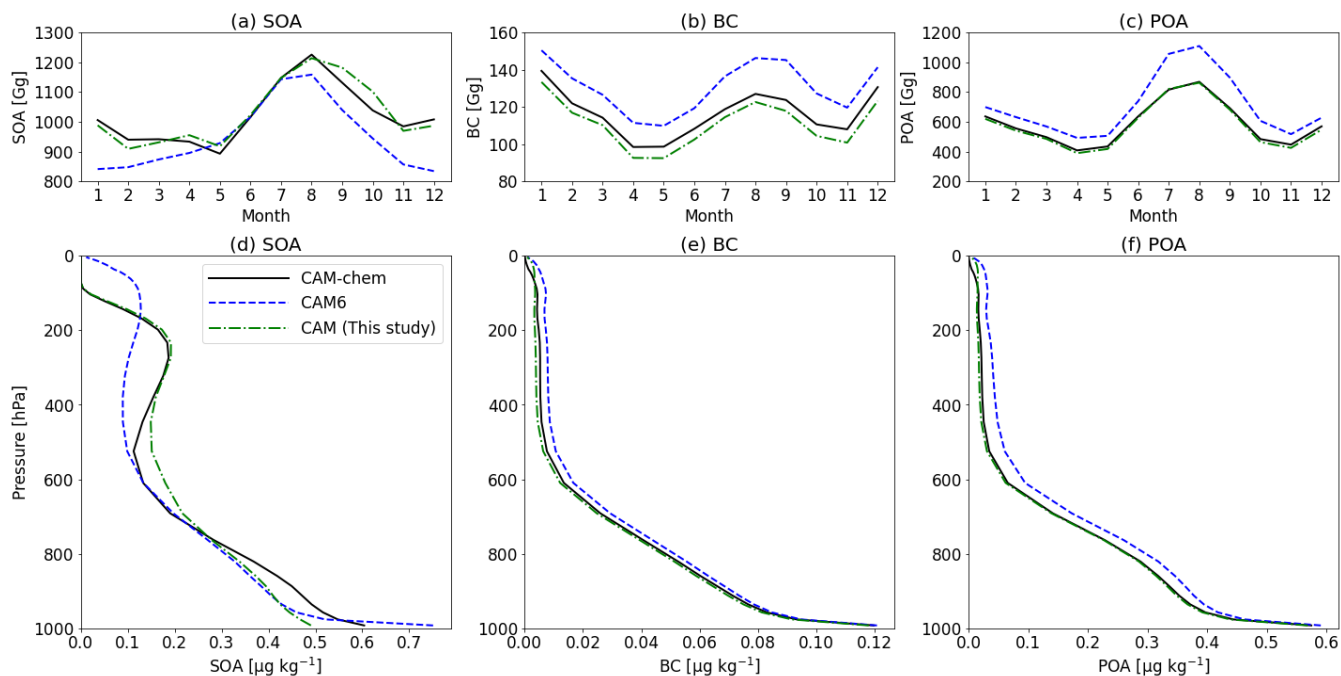
2000s - 1850s (SP)	CAM-chem	13	8	57	210	-0.98	-0.97	-0.01	-1.47	-0.54
	CAM6	97	0	60	200	-1.15	-1.04	-0.11	-1.67	-0.66
	CAM (This study)	-3	11	52	188	-0.98	-0.91	-0.07	-1.58	-0.70
2000s - 1850s (BGC)	CAM-chem	156	54	57	208	-0.92	-1.08	0.16	-1.31	-0.59
	CAM (This study)	182	19	52	185	-0.96	-0.97	0.01	-1.44	-0.75

### 290 3.1 Aerosols

291 Table 2 shows the global annual mean burden of aerosols by different simulations, including gas-  
292 phase SOA or semivolatiles (SOAG). Two CAM cases and CAM-chem are consistent within 10% in  
293 terms of global SOA burden, with the new scheme showing better agreement. SOAG is substantially  
294 underestimated in both CAM cases, because high volatility bins (saturation vapor pressure of  $10 \mu\text{g m}^{-3}$   
295 and  $100 \mu\text{g m}^{-3}$ ) are not simulated in the 1-bin simple SOA scheme. However, SOAG does not affect  
296 other aerosol concentrations and radiation fields, and therefore it is not an important species in CAM.

297 Although the two CAM cases show similar global SOA burdens to CAM-chem, their temporal and  
298 spatial distributions are very different. Figure 2 shows the monthly timeseries and mean vertical profile  
299 of the global SOA burden simulated by CAM and CAM-chem in 2013. In terms of reproducing CAM-  
300 chem SOA, the lower SOA during the Northern Hemisphere winter time and the SOA build-up in the  
301 upper atmosphere ( $< 100 \text{ hPa}$ ) are greatly improved in this study. There is still a discrepancy between  
302 CAM (this study) and CAM-chem such as SOA at around  $500 \text{ hPa}$  and at the surface (Fig. 2d), due to the  
303 limitation of using only one volatility bin in CAM (to reduce the computational cost). One fixed volatility  
304 bin with one enthalpy value cannot fully reproduce gas-phase semivolatiles simulated by five bins and  
305 the temperature dependency of volatility changes.

306



307

308 **Figure 2.** Monthly timeseries of global atmospheric burden (first row) and vertical distributions (second  
 309 row) of annual average SOA, BC, and POA simulated by CESM2.

310 Figure 3 shows the global spatial distribution of SOA at 100 hPa, 500 hPa, 850 hPa, and the surface  
 311 levels simulated by CAM-chem and CAM. In the CAM6 simulation, the main source regions (South  
 312 America and Africa) are well represented at the surface layer (Fig. 3k) but do not appear in the free  
 313 troposphere and above (panels b, e, and h). This is because the CAM6 SOA scheme generates  
 314 semivolatiles directly from the surface emissions while the CAM-chem SOA scheme needs more time  
 315 for VOC reactions to make semivolatiles, which can form SOA in the free troposphere. The intermediate  
 316 tracer (SOAE) in the CAM (this study) implicitly considers this process and successfully captures SOA  
 317 peaks in the free troposphere (panels c, f, and i).

318 In addition, the CAM6 SOA scheme fails to reproduce the sharp gradient of CAM-chem SOA above  
 319 200 hPa (Fig. 2d) and simulates too much SOA globally (Fig. 3b). The missing loss processes (deposition  
 320 of semivolatiles and photolytic loss of SOA) and higher temperature dependency (enthalpy) of saturation  
 321 vapor pressure result in more SOA in the CAM6 simulation. This problem is solved in the CAM SOA  
 322 scheme developed in this study (Fig. 3c).

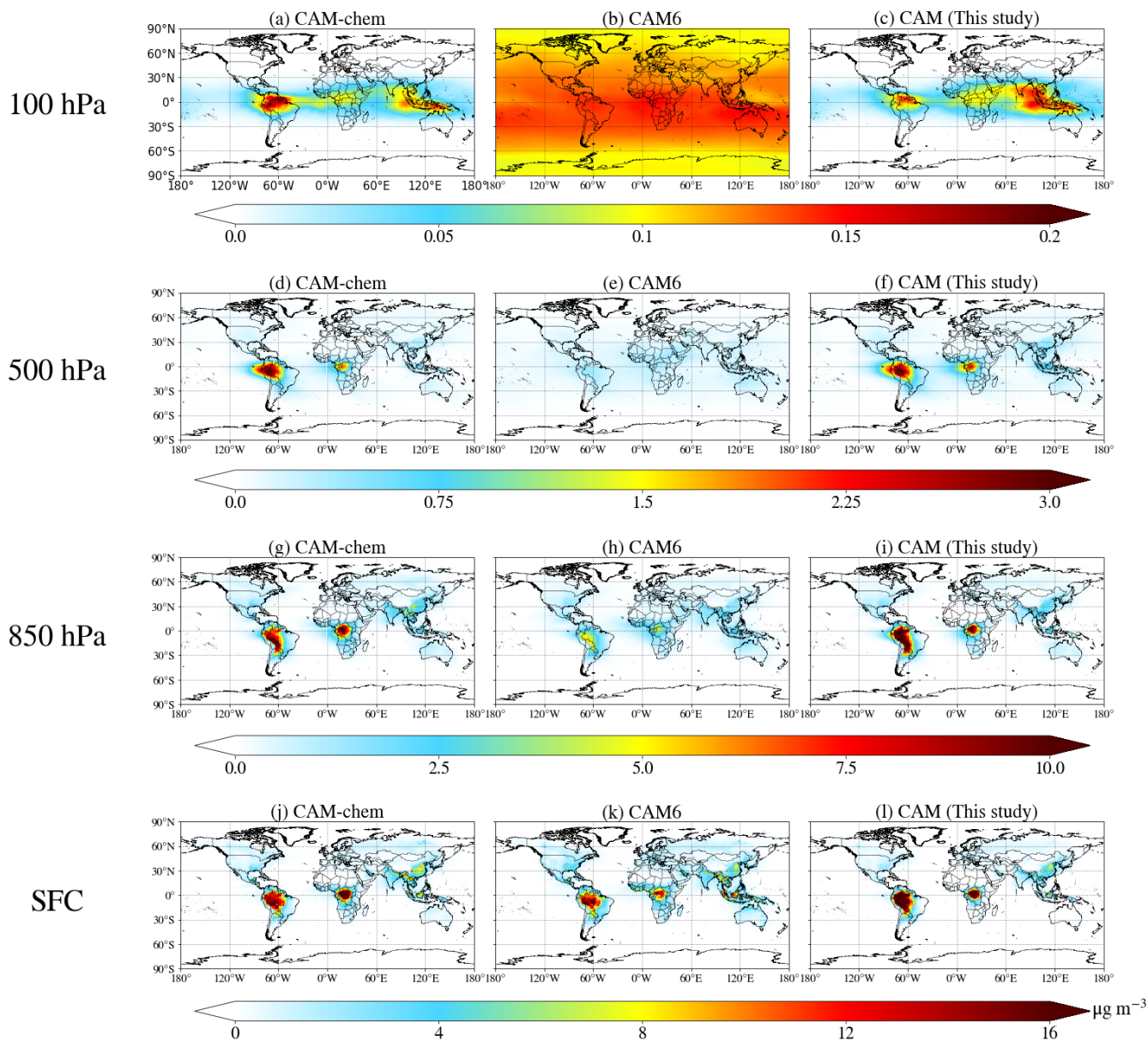


323 In order to quantitatively understand the relative importance of various components in the developed  
324 SOA scheme, six sensitivity simulations are conducted, as summarized in Table S1. Emission changes  
325 based on the CAM-chem VBS scheme, photolytic loss of SOA, and the intermediate tracer (SOAE) play  
326 significant roles in terms of SOA burden and similarities between CAM-chem and CAM compared to  
327 other changes made to the CAM SOA scheme described in Sect 2.3. In terms of the lifetime of SOA, both  
328 CAM-chem and CAM in this study show the same value (2.83 days) while CAM6 represents a longer  
329 lifetime (4.32 days). As a result, the fraction of grid cells within a factor of 2 and 5 compared to CAM-  
330 chem results are 62% and 82% using the CAM SOA scheme developed in this study, increased from 24%  
331 and 42% using the CAM6 scheme (Table S1). The shorter SOA lifetime in CAM-chem and CAM in this  
332 study is consistent with Hodzic et al. (2016).

333 Significant improvements are also found for BC and POA. CAM6 simulates up to ~45% differences  
334 while CAM in this study shows up to ~7% differences for BC and POA (Table 2). This is attributed to  
335 microphysical aging between different aerosol modes and associated wet deposition processes described  
336 in Sect 2.4. As discussed in Tilmes et al. (2019), the CAM6 SOA scheme simulates a higher primary  
337 carbon mode (41 and 276 Gg for BC and POA) compared to both CAM-chem (19 and 93 Gg) and the  
338 CAM SOA scheme in this study (14 and 81 Gg). Conversely, the CAM6 SOA scheme simulates a lower  
339 accumulation mode (90 and 429 Gg for BC and POA) compared to CAM-chem (97 and 494 Gg) and the  
340 CAM SOA scheme in this study (97 and 493 Gg).

341 Unlike SOA, seasonalities of BC and POA are well represented in the CAM6 (panels b and c in Fig.  
342 2), since BC and POA schemes are the same between CAM and CAM-chem. Spatial distributions are  
343 also similar (Figs. S3–S6) except for the Arctic regions in the upper atmosphere. This difference can  
344 significantly affect the radiation budget in the Arctic region (Sect. 3.2), which should be important for  
345 climate studies focusing on the Arctic.

346  
347  
348  
349



350

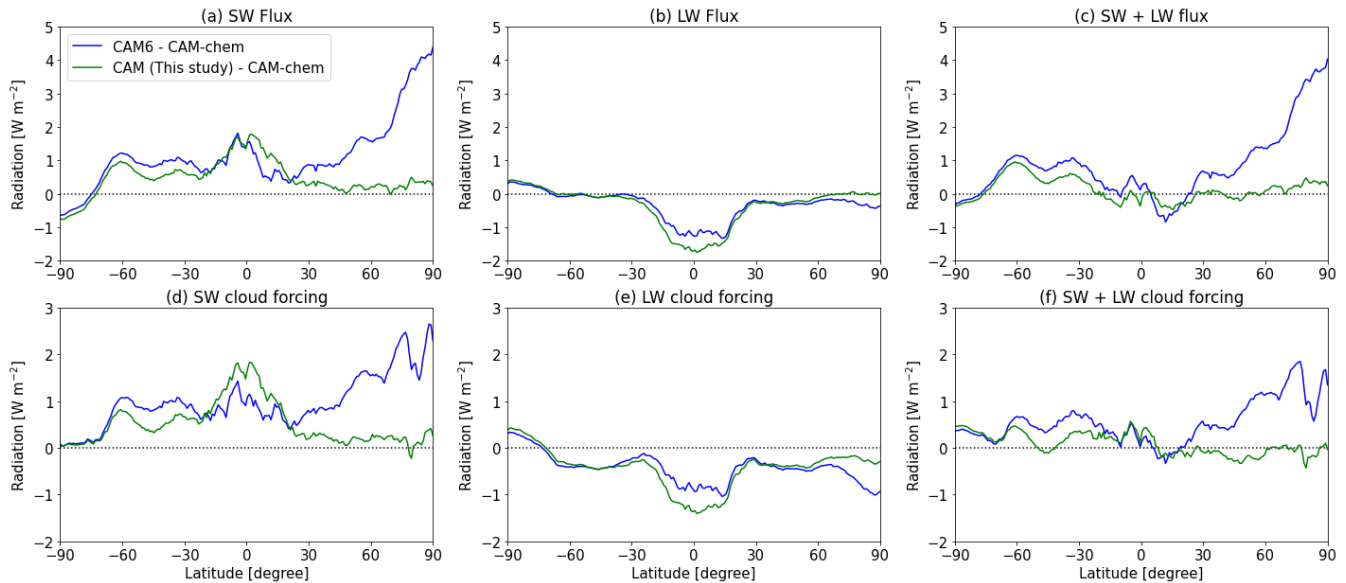
351 **Figure 3.** Global maps of SOA concentrations in 2013 simulated by CAM-chem (first column), CAM6  
 352 (second column), and CAM (This study) (third column) at four different vertical levels (surface, 850 hPa,  
 353 500 hPa, and 100 hPa). The difference maps between CAM and CAM-chem are available in Fig. S2.

354

355 **3.2 Radiation fields**

356 As aerosols can affect radiative fluxes through direct and indirect effects, here we investigate the  
 357 radiation changes with the SOA scheme developed in this study, in terms of the difference between CAM  
 358 and CAM-chem. Figure 4 shows the zonal averages of net shortwave (SW) and longwave (LW) fluxes  
 359 and cloud forcings in CAM compared to CAM-chem. The most notable differences occur in the high  
 360 latitudes in the Northern Hemisphere, similar to aerosol concentration changes shown in Sect 3.1. Both  
 361 aerosol-radiation and aerosol-cloud interactions almost equally contribute to the positive bias (panels a  
 362 and d). This strong positive bias of the SW flux in CAM6 is greatly improved with the SOA scheme  
 363 developed in this study.

364



365

366 **Figure 4.** Zonal averages of the radiation difference in 2013 between CAM and CAM-chem. Radiative  
 367 fluxes at the top of the model are presented in the first row (a-c) and cloud forcings are shown in the  
 368 second row (d-f).

369

370

371

372

373

374 The differences between CAM-chem and CAM are slightly increased over the Tropics for individual  
375 SW and LW fluxes, which are mainly caused by cloud effects as shown in Figs. 4d and 4e, but these  
376 differences are canceled out in terms of the total radiation (Figs. 4c and 4f). Overall, the SOA scheme in  
377 this study shows slight improvements in other latitudes in addition to the Arctic region when it comes to  
378 reproducing CAM-chem results. The reduced differences can be further confirmed by the global spatial  
379 distributions shown in Fig. S7, the CAM simulation in this study shows results closer to CAM-chem in  
380 most locations globally (panels h and i in Fig. S7).

381

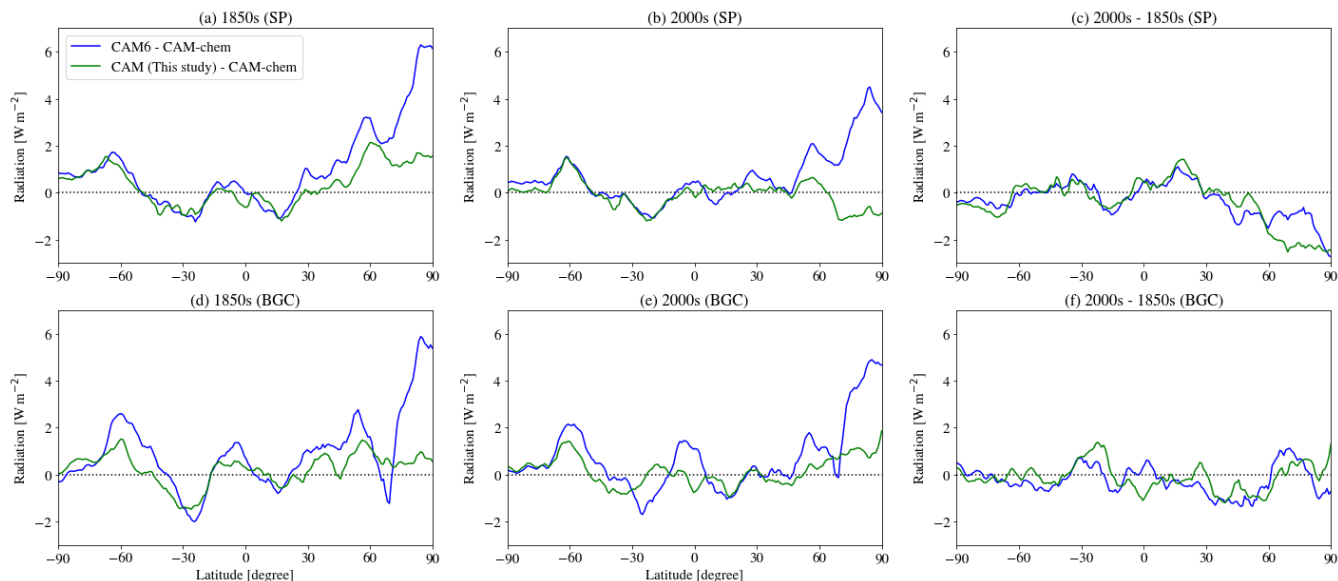
### 382 **3.3 Historical simulations**

383 Analogous to the simulation results with nudged meteorology in Sect 3.1 and 3.2, the SOA scheme  
384 in this study produces more consistent results with CAM-chem than the CAM6 SOA scheme (Table 2),  
385 especially for BC and POA burdens that are affected by SOA through microphysics. The new SOA  
386 scheme also captures the increased SOA burden in the 2000s compared to the 1850s when using the BGC  
387 option, which is mainly caused by increased biogenic VOC emissions (Fig. S8).

388 Figure S8 further shows that interannual variability may not be a significant factor for isoprene  
389 emissions on a 10-years time scale, but this would be important for climate studies with more than 100  
390 years of simulation time (1850s vs 2000s). The offline emissions used in CAM6 have no interannual  
391 variability, thus not accounting for emission response to climate change.

392 The large differences between CAM-chem and CAM6 for the SW + LW flux over the Arctic from  
393 the nudged meteorology simulations (Fig. 4c) are also found in all historical simulations as shown in Fig.  
394 5, for both 1850s and 2000s simulations. However, in terms of the difference between the 2000s and  
395 1850s, the biases cancel out, and as a result, the difference between CAM6 and CAM-chem becomes  
396 small (Figs. 5c and 5f). This cancellation implies that previous CAM studies focusing on radiative forcing  
397 are still valid, as radiative forcing is calculated as present minus preindustrial radiative effects.

398 In terms of global averages (Table 2), the CAM SOA scheme in this study also demonstrates  
 399 improvements in terms of consistency between CAM and CAM-chem, especially for shortwave radiation.  
 400 This applies to both absolute values and the difference between present and pre-industrial simulations.  
 401



402  
 403 **Figure 5.** Zonal averages of the SW + LW flux difference in historical simulations (1850s (a and d),  
 404 2000s (b and e), and 2000s - 1850s (c and f)) between CAM and CAM-chem. Note that the results from  
 405 the CAM6 simulations are the same for SP and BGC because CAM6 uses offline biogenic emissions.  
 406 CAM-chem and CAM (This study) results affect the difference between SP and BGC simulations (blue  
 407 lines).

#### 408 4 Conclusion and possible future developments of the aerosol scheme in CAM

409 In this study, we developed a new SOA scheme for use in CAM with simple chemistry. This new  
 410 SOA scheme was designed to close the gap between CAM and CAM-chem in terms of aerosols and  
 411 radiative effects while maintaining computational efficiency. The new SOA scheme was derived based  
 412 on the parameters used in the VBS scheme in CAM-chem, without changing the overall architecture of  
 413 the simple SOA scheme in CAM6. For instance, VOC species for forming SOA were matched to CAM-  
 414 chem, an intermediate species was introduced to mimic VOC chemistry, missing loss processes were  
 415 added, and VBS parameters such as enthalpy of vaporization and saturation vapor pressure were updated.

416 As a result, the computational cost remained almost the same with the new SOA scheme (within the range  
417 of computing environment variability).

418 CAM simulation results with the two SOA schemes (CAM6 and this study) were investigated in  
419 terms of carbonaceous aerosols and radiative fluxes. There was no significant bias in terms of the global  
420 SOA burden of the CAM6 SOA scheme because it was tuned by increasing SOA emissions by 50% (Liu  
421 et al., 2012). However, the CAM6 SOA scheme was insufficient in reproducing the temporal and spatial  
422 variabilities (both horizontally and vertically) of CAM-chem SOA, while the SOA scheme in this study  
423 demonstrated similar variabilities compared to CAM-chem SOA.

424 The new SOA scheme also improved the simulation of other carbonaceous aerosols (BC and POA)  
425 through the microphysical processes in MAM4. Since BC and POA emissions are the same for all model  
426 cases and those aerosols are chemically inert, temporal and horizontal spatial variabilities are generally  
427 similar to each other but the absolute concentrations became closer to CAM-chem results when using the  
428 new SOA scheme. The higher BC in CAM was greatly reduced compared to CAM-chem, from ~45% in  
429 the CAM6 SOA scheme to ~7% in the new SOA scheme. POA was also improved in the same manner.  
430 Major improvements were made in the Arctic region for aerosol concentrations in the free troposphere  
431 and above.

432 The improvements in simulating aerosol fields led to more consistent radiative fluxes between CAM  
433 and CAM-chem, especially over the high-latitude regions in the Northern Hemisphere. The SW + LW  
434 flux at the top of the model was different by up to  $6 \text{ W m}^{-2}$  and it is persistent regardless of the simulation  
435 periods in CAM6. However, in terms of radiative forcing which is calculated from the difference between  
436 present and pre-industrial conditions, both CAM6 and new CAM simulations showed no significant  
437 differences. While studies investigating instantaneous radiative effects will need to use the SOA scheme  
438 developed in this study, the CAM6 SOA scheme would still be valid for studies focusing on radiative  
439 forcing.

440 On the practical side, the new SOA scheme developed in this study has advantages in keeping up  
441 with the updates, as it uses the same precursor emissions as the VBS scheme in CAM-chem. The new  
442 SOA scheme uses online biogenic emissions as CAM-chem does, therefore the difference between SP

443 and BGC options can be calculated for SOA. If there is a future update in the VBS scheme in CAM-chem,  
444 the corresponding updates in CAM can be done easily by changing the namelist file.

445 Although significant advances have been made in SOA concentration simulation in this study, the  
446 aerosol module in CAM still has room for further development. Currently, CAM reads the offline monthly  
447 oxidant fields simulated by CAM-chem but oxidants such as OH and O<sub>3</sub> have strong diurnal variations. It  
448 would not be computationally feasible for CAM to calculate or read oxidants every hour, but applying  
449 constant diurnal profile values to the monthly fields would not add significant computational costs. It may  
450 be important for SO<sub>2</sub> oxidation and sulfate formation as well. The formation of SOAG from SOAE is  
451 calculated using a 1-day lifetime, but future versions could use the reaction rate constant with OH if the  
452 diurnal variation of oxidant fields is introduced in CAM. This improvement can be easily achieved by  
453 modifying the mechanism input file, however currently the prescribed OH fields are monthly means, so  
454 would provide limited improvement now.

455 Since there are many uncertainties in OA simulation in models, continuous updates to the CAM-  
456 chem VBS scheme will be necessary. As Hodzic et al. (2020) pointed out, CAM-chem showed good  
457 agreement in reproducing absolute OA concentrations during the Atmospheric Tomography (ATom)  
458 aircraft campaign, but the POA/SOA ratio was overestimated. CAM-chem considers SOA from S/IVOCs  
459 based on the assumption that the emission inventory they used reported POA emissions after evaporation  
460 to S/IVOCs (Hodzic et al., 2016). However, there is a possibility of double-counting depending on the  
461 timing of measuring POA emission flux. Additionally, the assumption that SVOC emissions were  
462 included in POA emissions was not sufficiently constrained due to limited observation data (Wu et al.,  
463 2019). Fang et al. (2021) reported that IVOCs did not show significant correlations with POA or  
464 NMVOCs for on-road vehicles. CAM-chem also assumes a single value for the organic mass to organic  
465 carbon (OM/OC) ratio of 1.4 for POA. In contrast, GEOS-Chem has used an OM/OC ratio of 2.1 for POA  
466 (Henze et al., 2008; Jo et al., 2013; Hodzic et al., 2020), which would lead to 50% higher POA  
467 concentrations than CAM-chem if other conditions are the same. However, observed OM/OC values are  
468 spatially and seasonally dependent, typically ranging from 1.3 to 2.5 (Aiken et al., 2008; Philip et al.,  
469 2014). These uncertain factors suggest that current assumptions about S/IVOCs and POA may need to be

470 updated in the future. Still, such updates in CAM-chem can be easily transferred into CAM through the  
471 consistent framework established in this study.

472 The SOA scheme in this study can be further adjusted depending on the research interest. For  
473 example, for studies focusing on surface aerosol fields, users can easily modify SOA yields for different  
474 emission sources through namelist changes. For studies focusing on urban air quality and resulting climate  
475 effects, SOA yields can be changed to high-NO<sub>x</sub> yields instead of low-NO<sub>x</sub> yields without code changes.  
476 Vertical shapes can be also adjusted by changing the parameters such as the enthalpy of vaporization,  
477 saturation vapor pressure, and photolysis rates in the future.

478

479 **Code and data availability.** CESM is an open-source community model and is publicly available at:  
480 <https://github.com/ESCOMP/CESM>. The new SOA scheme is included in the development version of the  
481 CAM (<https://github.com/ESCOMP/CAM>, tag name: cam6\_3\_093) and also available at Zenodo  
482 repository (<https://doi.org/10.5281/zenodo.7807711>), and will be publicly available in the next CESM  
483 release. The model results used in this study are available on Zenodo (TBD, will be updated with the final  
484 dataset after the completion of the review process).

485

486 **Author contributions.** DSJ, ST, and LKE designed the research and developed the SOA scheme. SW  
487 developed the OASISS scheme. DSJ, ST, and FV conducted CESM simulations. DSJ wrote the  
488 manuscript. All authors contributed to editing the manuscript.

489

490 **Competing interests.** The authors declare that they have no conflict of interest.

491

492 **Acknowledgments.** This material is based upon work supported by the National Center for Atmospheric  
493 Research, which is a major facility sponsored by the National Science Foundation (NSF) under  
494 Cooperative Agreement No. 1852977. This research was supported by NASA ACCDAM (award  
495 80NSSC21K1439). We would like to acknowledge high-performance computing support from Cheyenne  
496 (doi:10.5065/D6RX99HX) provided by NCAR's Computational and Information Systems Laboratory,



497 sponsored by the NSF. The authors thank Behrooz Roozitalab and Alma Hodzic (NCAR) for their  
498 valuable comments on the manuscript.  
499

500 **References**

- 501 Aiken, A. C., Decarlo, P. F., Kroll, J. H., Worsnop, D. R., Huffman, J. A., Docherty, K. S., Ulbrich, I.  
502 M., Mohr, C., Kimmel, J. R., Sueper, D., Sun, Y., Zhang, Q., Trimborn, A., Northway, M., Ziemann, P.  
503 J., Canagaratna, M. R., Onasch, T. B., Alfarra, M. R., Prevot, A. S. H., Dommen, J., Duplissy, J.,  
504 Metzger, A., Baltensperger, U. and Jimenez, J. L.: O/C and OM/OC ratios of primary, secondary, and  
505 ambient organic aerosols with high-resolution time-of-flight aerosol mass spectrometry, *Environ. Sci.*  
506 *Technol.*, 42(12), 4478–4485, doi:10.1021/es703009q, 2008.
- 507 Danabasoglu, G., Lamarque, J. -F, Bacmeister, J., Bailey, D. A., DuVivier, A. K., Edwards, J.,  
508 Emmons, L. K., Fasullo, J., Garcia, R., Gettelman, A., Hannay, C., Holland, M. M., Large, W. G.,  
509 Lauritzen, P. H., Lawrence, D. M., Lenaerts, J. T. M., Lindsay, K., Lipscomb, W. H., Mills, M. J.,  
510 Neale, R., Oleson, K. W., Otto-Bliesner, B., Phillips, A. S., Sacks, W., Tilmes, S., Kampenhout, L.,  
511 Vertenstein, M., Bertini, A., Dennis, J., Deser, C., Fischer, C., Fox-Kemper, B., Kay, J. E., Kinnison,  
512 D., Kushner, P. J., Larson, V. E., Long, M. C., Mickelson, S., Moore, J. K., Nienhouse, E., Polvani, L.,  
513 Rasch, P. J. and Strand, W. G.: The community earth system model version 2 (CESM2), *J. Adv. Model.*  
514 *Earth Syst.*, 12(2), doi:10.1029/2019ms001916, 2020.
- 515 Donahue, N. M., Robinson, A. L., Stanier, C. O. and Pandis, S. N.: Coupled partitioning, dilution, and  
516 chemical aging of semivolatile organics, *Environ. Sci. Technol.*, 40(8), 2635–2643,  
517 doi:10.1021/es052297c, 2006.
- 518 Donahue, N. M., Epstein, S. A., Pandis, S. N. and Robinson, A. L.: A two-dimensional volatility basis  
519 set: 1. organic-aerosol mixing thermodynamics, *Atmos. Chem. Phys.*, 11(7), 3303–3318,  
520 doi:10.5194/acp-11-3303-2011, 2011.
- 521 Donahue, N. M., Kroll, J. H., Pandis, S. N. and Robinson, A. L.: A two-dimensional volatility basis set  
522 – Part 2: Diagnostics of organic-aerosol evolution, *Atmos. Chem. Phys.*, 12(2), 615–634,  
523 doi:10.5194/acp-12-615-2012, 2012.
- 524 Emmons, L. K., Schwantes, R. H., Orlando, J. J., Tyndall, G., Kinnison, D., Lamarque, J., Marsh, D.,  
525 Mills, M. J., Tilmes, S., Bardeen, C., Buchholz, R. R., Conley, A., Gettelman, A., Garcia, R., Simpson,  
526 I., Blake, D. R., Meinardi, S. and Pétron, G.: The chemistry mechanism in the community earth system  
527 model version 2 (CESM2), *J. Adv. Model. Earth Syst.*, 12(4), e2019MS001882,  
528 doi:10.1029/2019ms001882, 2020.
- 529 Epstein, S. A., Riipinen, I. and Donahue, N. M.: A semiempirical correlation between enthalpy of  
530 vaporization and saturation concentration for organic aerosol, *Environ. Sci. Technol.*, 44(2), 743–748,  
531 doi:10.1021/es902497z, 2010.
- 532 Fang, H., Huang, X., Zhang, Y., Pei, C., Huang, Z., Wang, Y., Chen, Y., Yan, J., Zeng, J., Xiao, S.,  
533 Luo, S., Li, S., Wang, J., Zhu, M., Fu, X., Wu, Z., Zhang, R., Song, W., Zhang, G., Hu, W., Tang, M.,

- 534 Ding, X., Bi, X. and Wang, X.: Measurement report: Emissions of intermediate-volatility organic  
535 compounds from vehicles under real-world driving conditions in an urban tunnel, *Atmos. Chem. Phys.*,  
536 21(13), 10005–10013, doi:10.5194/acp-21-10005-2021, 2021.
- 537 Gelaro, R., McCarty, W., Suárez, M. J., Todling, R., Molod, A., Takacs, L., Randles, C., Darmenov, A.,  
538 Bosilovich, M. G., Reichle, R., Wargan, K., Coy, L., Cullather, R., Draper, C., Akella, S., Buchard, V.,  
539 Conaty, A., da Silva, A., Gu, W., Kim, G.-K., Koster, R., Lucchesi, R., Merkova, D., Nielsen, J. E.,  
540 Partyka, G., Pawson, S., Putman, W., Rienecker, M., Schubert, S. D., Sienkiewicz, M. and Zhao, B.:  
541 The Modern-Era Retrospective Analysis for Research and Applications, Version 2 (MERRA-2), *J.*  
542 *Clim.*, 30(Iss 13), 5419–5454, doi:10.1175/JCLI-D-16-0758.1, 2017.
- 543 Gettelman, A. and Morrison, H.: Advanced Two-Moment Bulk Microphysics for Global Models. Part I:  
544 Off-Line Tests and Comparison with Other Schemes, *J. Clim.*, 28(3), 1268–1287, doi:10.1175/JCLI-D-  
545 14-00102.1, 2015.
- 546 Gettelman, A., Hannay, C., Bacmeister, J. T., Neale, R. B., Pendergrass, A. G., Danabasoglu, G.,  
547 Lamarque, J. -F, Fasullo, J. T., Bailey, D. A., Lawrence, D. M. and Mills, M. J.: High Climate  
548 Sensitivity in the Community Earth System Model Version 2 (CESM2), *Geophys. Res. Lett.*, 46(14),  
549 8329–8337, doi:10.1029/2019GL083978, 2019a.
- 550 Gettelman, A., Mills, M. J., Kinnison, D. E., Garcia, R. R., Smith, A. K., Marsh, D. R., Tilmes, S., Vitt,  
551 F., Bardeen, C. G., McInerny, J., Liu, H.-L., Solomon, S. C., Polvani, L. M., Emmons, L. K., Lamarque,  
552 J.-F., Richter, J. H., Glanville, A. S., Bacmeister, J. T., Phillips, A. S., Neale, R. B., Simpson, I. R.,  
553 DuVivier, A. K., Hodzic, A. and Randel, W. J.: The whole atmosphere community climate model  
554 version 6 (WACCM6), *J. Geophys. Res.*, 124(23), 12380–12403, doi:10.1029/2019jd030943, 2019b.
- 555 Goldstein, A. H. and Galbally, I. E.: Known and unexplored organic constituents in the earth's  
556 atmosphere, *Environ. Sci. Technol.*, 41(5), 1514–1521, doi:10.1021/es072476p, 2007.
- 557 Guenther, A. B., Jiang, X., Heald, C. L., Sakulyanontvittaya, T., Duhl, T., Emmons, L. K. and Wang,  
558 X.: The Model of Emissions of Gases and Aerosols from Nature version 2.1 (MEGAN2.1): an extended  
559 and updated framework for modeling biogenic emissions, *Geoscientific Model Development*, 5(6),  
560 1471–1492, doi:10.5194/gmd-5-1471-2012, 2012.
- 561 Hallquist, M., Wenger, J. C., Baltensperger, U., Rudich, Y., Simpson, D., Claeys, M., Dommen, J.,  
562 Donahue, N. M., George, C., Goldstein, A. H., Hamilton, J. F., Herrmann, H., Hoffmann, T., Iinuma,  
563 Y., Jang, M., Jenkin, M. E., Jimenez, J. L., Kiendler-Scharr, A., Maenhaut, W., McFiggans, G., Mentel,  
564 T. F., Monod, A., Prévôt, A. S. H., Seinfeld, J. H., Surratt, J. D., Szmigielski, R. and Wildt, J.: The  
565 formation, properties and impact of secondary organic aerosol: current and emerging issues, *Atmos.*  
566 *Chem. Phys.*, 9(14), 5155–5236, doi:10.5194/acp-9-5155-2009, 2009.
- 567 Henze, D. K., Seinfeld, J. H., Ng, N. L., Kroll, J. H., Fu, T.-M., Jacob, D. J. and Heald, C. L.: Global  
568 modeling of secondary organic aerosol formation from aromatic hydrocarbons: high- vs. low-yield

569 pathways, *Atmos. Chem. Phys.*, 8(9), 2405–2420, doi:10.5194/acp-8-2405-2008, 2008.

570 Hodzic, A., Kasibhatla, P. S., Jo, D. S., Cappa, C. D., Jimenez, J. L., Madronich, S. and Park, R. J.:  
571 Rethinking the global secondary organic aerosol (SOA) budget: stronger production, faster removal,  
572 shorter lifetime, *Atmos. Chem. Phys.*, 16(12), 7917–7941, doi:10.5194/acp-16-7917-2016, 2016.

573 Hodzic, A., Campuzano-Jost, P., Bian, H., Chin, M., Colarco, P. R., Day, D. A., Froyd, K. D., Heinold,  
574 B., Jo, D. S., Katich, J. M., Kodros, J. K., Nault, B. A., Pierce, J. R., Ray, E., Schacht, J., Schill, G. P.,  
575 Schroder, J. C., Schwarz, J. P., Sueper, D. T., Tegen, I., Tilmes, S., Tsigaridis, K., Yu, P. and Jimenez,  
576 J. L.: Characterization of organic aerosol across the global remote troposphere: a comparison of ATom  
577 measurements and global chemistry models, *Atmos. Chem. Phys.*, 20(8), 4607–4635, doi:10.5194/acp-  
578 20-4607-2020, 2020.

579 Hulswar, S., Simó, R., Galí, M., Bell, T. G., Lana, A., Inamdar, S., Halloran, P. R., Manville, G. and  
580 Mahajan, A. S.: Third revision of the global surface seawater dimethyl sulfide climatology (DMS-  
581 Rev3), *Earth Syst. Sci. Data*, 14(7), 2963–2987, doi:10.5194/essd-14-2963-2022, 2022.

582 Jimenez, J. L., Canagaratna, M. R., Donahue, N. M., Prevot, A. S. H., Zhang, Q., Kroll, J. H., DeCarlo,  
583 P. F., Allan, J. D., Coe, H., Ng, N. L., Aiken, A. C., Docherty, K. S., Ulbrich, I. M., Grieshop, A. P.,  
584 Robinson, A. L., Duplissy, J., Smith, J. D., Wilson, K. R., Lanz, V. A., Hueglin, C., Sun, Y. L., Tian, J.,  
585 Laaksonen, A., Raatikainen, T., Rautiainen, J., Vaattovaara, P., Ehn, M., Kulmala, M., Tomlinson, J.  
586 M., Collins, D. R., Cubison, M. J., Dunlea, E. J., Huffman, J. A., Onasch, T. B., Alfarra, M. R.,  
587 Williams, P. I., Bower, K., Kondo, Y., Schneider, J., Drewnick, F., Borrmann, S., Weimer, S.,  
588 Demerjian, K., Salcedo, D., Cottrell, L., Griffin, R., Takami, A., Miyoshi, T., Hatakeyama, S.,  
589 Shimono, A., Sun, J. Y., Zhang, Y. M., Dzepina, K., Kimmel, J. R., Sueper, D., Jayne, J. T., Herndon,  
590 S. C., Trimborn, A. M., Williams, L. R., Wood, E. C., Middlebrook, A. M., Kolb, C. E., Baltensperger,  
591 U. and Worsnop, D. R.: Evolution of organic aerosols in the atmosphere, *Science*, 326(5959), 1525–  
592 1529, doi:10.1126/science.1180353, 2009.

593 Jo, D. S., Park, R. J., Kim, M. J. and Spracklen, D. V.: Effects of chemical aging on global secondary  
594 organic aerosol using the volatility basis set approach, *Atmos. Environ.*, 81, 230–244,  
595 doi:10.1016/j.atmosenv.2013.08.055, 2013.

596 Jo, D. S., Hodzic, A., Emmons, L. K., Marais, E. A., Peng, Z., Nault, B. A., Hu, W., Campuzano-Jost,  
597 P. and Jimenez, J. L.: A simplified parameterization of isoprene-epoxydiol-derived secondary organic  
598 aerosol (IEPOX-SOA) for global chemistry and climate models: a case study with GEOS-Chem v11-  
599 02-rc, *Geoscientific Model Development*, 12(7), 2983–3000, doi:10.5194/gmd-12-2983-2019, 2019.

600 Jo, D. S., Hodzic, A., Emmons, L. K., Tilmes, S., Schwantes, R. H., Mills, M. J., Campuzano-Jost, P.,  
601 Hu, W., Zaveri, R. A., Easter, R. C., Singh, B., Lu, Z., Schulz, C., Schneider, J., Shilling, J. E.,  
602 Wisthaler, A. and Jimenez, J. L.: Future changes in isoprene-epoxydiol-derived secondary organic  
603 aerosol (IEPOX SOA) under the Shared Socioeconomic Pathways: the importance of physicochemical  
604 dependency, *Atmos. Chem. Phys.*, 21(5), 3395–3425, doi:10.5194/acp-21-3395-2021, 2021.

- 605 Lana, A., Bell, T. G., Simó, R., Vallina, S. M., Ballabrera-Poy, J., Kettle, A. J., Dachs, J., Bopp, L.,  
606 Saltzman, E. S. and Stefels, J.: An updated climatology of surface dimethylsulfide concentrations and  
607 emission fluxes in the global ocean, *Global Biogeochem. Cycles*, 25(1), doi:10.1029/2010GB003850,  
608 2011.
- 609 Lawrence, D. M., Fisher, R. A., Koven, C. D., Oleson, K. W., Swenson, S. C., Bonan, G., Collier, N.,  
610 Ghimire, B., Kampenhout, L., Kennedy, D., Kluzek, E., Lawrence, P. J., Li, F., Li, H., Lombardozzi,  
611 D., Riley, W. J., Sacks, W. J., Shi, M., Vertenstein, M., Wieder, W. R., Xu, C., Ali, A. A., Badger, A.  
612 M., Bisht, G., Broeke, M., Brunke, M. A., Burns, S. P., Buzan, J., Clark, M., Craig, A., Dahlin, K.,  
613 Drewniak, B., Fisher, J. B., Flanner, M., Fox, A. M., Gentine, P., Hoffman, F., Keppel-Aleks, G., Knox,  
614 R., Kumar, S., Lenaerts, J., Leung, L. R., Lipscomb, W. H., Lu, Y., Pandey, A., Pelletier, J. D., Perket,  
615 J., Randerson, J. T., Ricciuto, D. M., Sanderson, B. M., Slater, A., Subin, Z. M., Tang, J., Thomas, R.  
616 Q., Val Martin, M. and Zeng, X.: The community land model version 5: Description of new features,  
617 benchmarking, and impact of forcing uncertainty, *J. Adv. Model. Earth Syst.*, 11(12), 4245–4287,  
618 doi:10.1029/2018ms001583, 2019.
- 619 Lim, Y. B. and Ziemann, P. J.: Effects of molecular structure on aerosol yields from OH radical-  
620 initiated reactions of linear, branched, and cyclic alkanes in the presence of NO<sub>x</sub>, *Environ. Sci.*  
621 *Technol.*, 43(7), 2328–2334, doi:10.1021/es803389s, 2009.
- 622 Liu, X., Easter, R. C., Ghan, S. J., Zaveri, R., Rasch, P., Shi, X., Lamarque, J.-F., Gettelman, A.,  
623 Morrison, H., Vitt, F., Conley, A., Park, S., Neale, R., Hannay, C., Ekman, A. M. L., Hess, P.,  
624 Mahowald, N., Collins, W., Iacono, M. J., Bretherton, C. S., Flanner, M. G. and Mitchell, D.: Toward a  
625 minimal representation of aerosols in climate models: description and evaluation in the Community  
626 Atmosphere Model CAM5, *Geoscientific Model Development*, 5(3), 709–739, doi:10.5194/gmd-5-709-  
627 2012, 2012.
- 628 Liu, X., Ma, P.-L., Wang, H., Tilmes, S., Singh, B., Easter, R. C., Ghan, S. J. and Rasch, P. J.:  
629 Description and evaluation of a new four-mode version of the Modal Aerosol Module (MAM4) within  
630 version 5.3 of the Community Atmosphere Model, *Geoscientific Model Development*, 9(2), 505–522,  
631 doi:10.5194/gmd-9-505-2016, 2016.
- 632 Nault, B. A., Jo, D. S., McDonald, B. C., Campuzano-Jost, P., Day, D. A., Hu, W., Schroder, J. C.,  
633 Allan, J., Blake, D. R., Canagaratna, M. R., Coe, H., Coggon, M. M., DeCarlo, P. F., Diskin, G. S.,  
634 Dunmore, R., Flocke, F., Fried, A., Gilman, J. B., Gkatzelis, G., Hamilton, J. F., Hanisco, T. F., Hayes,  
635 P. L., Henze, D. K., Hodzic, A., Hopkins, J., Hu, M., Huey, L. G., Jobson, B. T., Kuster, W. C., Lewis,  
636 A., Li, M., Liao, J., Nawaz, M. O., Pollack, I. B., Peischl, J., Rappenglück, B., Reeves, C. E., Richter,  
637 D., Roberts, J. M., Ryerson, T. B., Shao, M., Sommers, J. M., Walega, J., Warneke, C., Weibring, P.,  
638 Wolfe, G. M., Young, D. E., Yuan, B., Zhang, Q., de Gouw, J. A. and Jimenez, J. L.: Secondary organic  
639 aerosols from anthropogenic volatile organic compounds contribute substantially to air pollution  
640 mortality, *Atmos. Chem. Phys.*, 21(14), 11201–11224, doi:10.5194/acp-21-11201-2021, 2021.
- 641 Neu, J. L. and Prather, M. J.: Toward a more physical representation of precipitation scavenging in

- 642 global chemistry models: cloud overlap and ice physics and their impact on tropospheric ozone, *Atmos.*  
643 *Chem. Phys.*, 12(7), 3289–3310, doi:10.5194/acp-12-3289-2012, 2012.
- 644 Oak, Y. J., Park, R. J., Jo, D. S., Hodzic, A., Jimenez, J. L., Campuzano-Jost, P., Nault, B. A., Kim, H.,  
645 Kim, H., Ha, E. S., Song, C.-K., Yi, S.-M., Diskin, G. S., Weinheimer, A. J., Blake, D. R., Wisthaler,  
646 A., Shim, M. and Shin, Y.: Evaluation of secondary organic aerosol (SOA) simulations for Seoul,  
647 Korea, *J. Adv. Model. Earth Syst.*, doi:10.1029/2021ms002760, 2022.
- 648 Philip, S., Martin, R. V., Pierce, J. R., Jimenez, J. L., Zhang, Q., Canagaratna, M. R., Spracklen, D. V.,  
649 Nowlan, C. R., Lamsal, L. N., Cooper, M. J. and Krotkov, N. A.: Spatially and seasonally resolved  
650 estimate of the ratio of organic mass to organic carbon, *Atmos. Environ.*, 87, 34–40,  
651 doi:10.1016/j.atmosenv.2013.11.065, 2014.
- 652 Robinson, A. L., Donahue, N. M., Shrivastava, M. K., Weitkamp, E. A., Sage, A. M., Grieshop, A. P.,  
653 Lane, T. E., Pierce, J. R. and Pandis, S. N.: Rethinking organic aerosols: semivolatile emissions and  
654 photochemical aging, *Science*, 315(5816), 1259–1262, doi:10.1126/science.1133061, 2007.
- 655 Schwantes, R. H., Lacey, F. G., Tilmes, S., Emmons, L. K., Lauritzen, P. H., Walters, S., Callaghan, P.,  
656 Zarzycki, C. M., Barth, M. C., Jo, D. S., Bacmeister, J. T., Neale, R. B., Vitt, F., Kluzek, E., Roozitalab,  
657 B., Hall, S. R., Ullmann, K., Warneke, C., Peischl, J., Pollack, I. B., Flocke, F., Wolfe, G. M., Hanisco,  
658 T. F., Keutsch, F. N., Kaiser, J., Bui, T. P. V., Jimenez, J. L., Campuzano-Jost, P., Apel, E. C.,  
659 Hornbrook, R. S., Hills, A. J., Yuan, B. and Wisthaler, A.: Evaluating the impact of chemical  
660 complexity and horizontal resolution on tropospheric ozone over the conterminous US with a global  
661 variable resolution chemistry model, *J. Adv. Model. Earth Syst.*, doi:10.1029/2021ms002889, 2022.
- 662 Shan, Y., Liu, X., Lin, L., Ke, Z. and Lu, Z.: An improved representation of aerosol wet removal by  
663 deep convection and impacts on simulated aerosol vertical profiles, *J. Geophys. Res.*, 126(13),  
664 doi:10.1029/2020jd034173, 2021.
- 665 Sporre, M. K., Blichner, S. M., Karset, I. H. H., Makkonen, R. and Berntsen, T. K.: BVOC–aerosol–  
666 climate feedbacks investigated using NorESM, *Atmos. Chem. Phys.*, 19(7), 4763–4782,  
667 doi:10.5194/acp-19-4763-2019, 2019.
- 668 Srivastava, D., Vu, T. V., Tong, S., Shi, Z. and Harrison, R. M.: Formation of secondary organic  
669 aerosols from anthropogenic precursors in laboratory studies, *npj Climate and Atmospheric Science*,  
670 5(1), 1–30, doi:10.1038/s41612-022-00238-6, 2022.
- 671 Tilmes, S., Hodzic, A., Emmons, L. K., Mills, M. J., Gettelman, A., Kinnison, D. E., Park, M.,  
672 Lamarque, J. -F, Vitt, F., Shrivastava, M., Campuzano-Jost, P., Jimenez, J. L. and Liu, X.: Climate  
673 Forcing and Trends of Organic Aerosols in the Community Earth System Model (CESM2), *J. Adv.*  
674 *Model. Earth Syst.*, 18, 17,745, doi:10.1029/2019MS001827, 2019.
- 675 Tsigaridis, K. and Kanakidou, M.: The Present and Future of Secondary Organic Aerosol Direct

- 676 Forcing on Climate, *Current Climate Change Reports*, 4(2), 84–98, doi:10.1007/s40641-018-0092-3,  
677 2018.
- 678 Wang, H., Easter, R. C., Rasch, P. J., Wang, M., Liu, X., Ghan, S. J., Qian, Y., Yoon, J.-H., Ma, P.-L.  
679 and Vinoj, V.: Sensitivity of remote aerosol distributions to representation of cloud–aerosol interactions  
680 in a global climate model, *Geosci. Model Dev.*, 6(3), 765–782, doi:10.5194/gmd-6-765-2013, 2013.
- 681 Wang, S., Hornbrook, R. S., Hills, A., Emmons, L. K., Tilmes, S., Lamarque, J., Jimenez, J. L.,  
682 Campuzano-Jost, P., Nault, B. A., Crouse, J. D., Wennberg, P. O., Kim, M., Allen, H., Ryerson, T. B.,  
683 Thompson, C. R., Peischl, J., Moore, F., Nance, D., Hall, B., Elkins, J., Tanner, D., Huey, L. G., Hall, S.  
684 R., Ullmann, K., Orlando, J. J., Tyndall, G. S., Flocke, F. M., Ray, E., Hanisco, T. F., Wolfe, G. M., St.  
685 Clair, J., Commane, R., Daube, B., Barletta, B., Blake, D. R., Weinzierl, B., Dollner, M., Conley, A.,  
686 Vitt, F., Wofsy, S. C., Riemer, D. D. and Apel, E. C.: Atmospheric Acetaldehyde: Importance of Air-  
687 Sea Exchange and a Missing Source in the Remote Troposphere, *Geophys. Res. Lett.*, 46(10), 5601–  
688 5613, doi:10.1029/2019GL082034, 2019.
- 689 Wang, S., Apel, E. C., Schwantes, R. H., Bates, K. H., Jacob, D. J., Fischer, E. V., Hornbrook, R. S.,  
690 Hills, A. J., Emmons, L. K., Pan, L. L., Honomichl, S., Tilmes, S., Lamarque, J.-F., Yang, M.,  
691 Marandino, C. A., Saltzman, E. S., de Bruyn, W., Kameyama, S., Tanimoto, H., Omori, Y., Hall, S. R.,  
692 Ullmann, K., Ryerson, T. B., Thompson, C. R., Peischl, J., Daube, B. C., Commane, R., McKain, K.,  
693 Sweeney, C., Thames, A. B., Miller, D. O., Brune, W. H., Diskin, G. S., DiGangi, J. P. and Wofsy, S.  
694 C.: Global atmospheric budget of acetone: Air-sea exchange and the contribution to hydroxyl radicals,  
695 *J. Geophys. Res.*, 125(15), doi:10.1029/2020jd032553, 2020.
- 696 Warneck, P. and Williams, J.: *The Atmospheric Chemist’s Companion: Numerical Data for Use in the*  
697 *Atmospheric Sciences*, Springer Netherlands, <http://dx.doi.org/10.1007/978-94-007-2275-0>, 2014.
- 698 Wu, L., Wang, X., Lu, S., Shao, M. and Ling, Z.: Emission inventory of semi-volatile and intermediate-  
699 volatility organic compounds and their effects on secondary organic aerosol over the Pearl River Delta  
700 region, *Atmos. Chem. Phys.*, 19(12), 8141–8161, doi:10.5194/acp-19-8141-2019, 2019.
- 701 Zhang, G. J. and McFarlane, N. A.: Sensitivity of climate simulations to the parameterization of  
702 cumulus convection in the Canadian climate centre general circulation model, *Atmosphere-Ocean*,  
703 33(3), 407–446, doi:10.1080/07055900.1995.9649539, 1995.
- 704 Zhang, L., Gong, S., Padro, J. and Barrie, L.: A size-segregated particle dry deposition scheme for an  
705 atmospheric aerosol module, *Atmos. Environ.*, 35(3), 549–560, doi:10.1016/S1352-2310(00)00326-5,  
706 2001.